XIII SIMMEC
Simpósio de Mecânica Computacional
29 de Outubro a 1º de Novembro de 2018
UFES - Campus Goiabeiras - Vitória, ES

The effects of different volume fraction distribution and micromechanics homogenization schemes on the mechanical behavior of FGM pressurized pipes

Marcelo Silva Medeiros Jr. (1); Evandro Parente Jr. (1); Antônio Macário Cartaxo de Melo (1)

(1), Universidade Federal do Ceará, Fortaleza - CE, Brasil.

Abstract: Functionally Graded Materials are characterized by a smooth and gradual microstructural composition along one or more of its dimensions. Problems related to the existence of interfaces such as debonding and delaminations, which are commonplace in laminated composites, are mitigated in such materials. FGMs are manufactured by varying the volume fraction of its constituents throughout its thickness, in order to tailor the final mechanical properties. Micromechanics homogenization schemes have been successfully employed on the study of these materials to obtain a description of the constitutive laws that describe the macroscopic state of stress and strain as a function of the microstructural composition. Such methods can be either analytical or numerical, but both approaches take into account the influence of the several phases or inclusions on the overall behavior of a representative volume element (RVE). The analysis of the differences among various homogenization schemes, different volume fraction profiles, as well as the influence of the inclusion geometry on the overall behavior of the FGM thick cylinder was carried out in the present work. The composite chosen for the analysis was Al-SiC and the comparisons were made in terms of stress and strain profiles along the wall of a pressurized hollow cylinder with varying SiC profiles. User subroutines (UMAT) were developed in Abaqus in which different homogenization schemes were implemented and analyzed. The results found showed the importance of the accurately describing the volume fraction distribution as well as the impact of the different homogenization schemes on the overall mechanical behavior of the material.

Keywords: *Micromechanics; Homogenization; FGM, UMAT.*

1 INTRODUCTION

Metal Matrix Composites (MMCs) combine the ductility and toughness of metals with the high strength, high modulus and low thermal conductivity of ceramics. This combination of qualities leads to materials with a superior thermomechanical performance. The use of MMCs as a major component in aerospace, automotive, maritime and petroleum industries has been established over the recent years. This was the result of the widespread availability of relatively inexpensive reinforcements, especially particulates in the micro and nano scales. Additionally, the development of various processing and manufacturing technologies resulted in reproducible microstructures and final products with more compliant properties.

Reduction in structural weight can be achieved, not only by reducing the alloy's density, but also by increasing its modulus and strength. For example, an increase in modulus, attained by substituting a wrought aluminum part by a particulate reinforced aluminum alloy, can result in overall weight reduction [1]. Reinforcement may be in the form of continuous fibers, chopped fibers, whiskers, platelets, or particulates. Common reinforcement particulates include, but are not restricted to, carbides (e.g., SiC, B_4C), nitrides (e.g., Si_3N_4, AlN), oxides (e.g., Al_20_3, SiO_2), as well as elemental materials (e.g., C, Si). Silicon Carbide, (SiC), for example, is a particulate powder that is commonly used in aluminum and magnesium MMCs.

The demand for a high performance thermal barrier to withstand the elevated temperatures from space vehicles re-entries, originated a new class of composites called functionally graded materials (FGMs) [2]. Functionally graded materials are essentially a class of advanced composites formed by two or more constituent phases (matrix and inclusions) with a gradual and continuously varying microstructural composition. That leads to structural elements with different functional performance within different sections of the same part. The technologies to produce FGM composites have not reached their maturity yet and are expected to have an ever-growing impact on the design and development of new components and structures in the years to come.

There are currently several different approaches to successfully introduce ceramic particulates into and alloy melt. Processes such as, injection of powders entrained in an inert gas, addition of particles by mechanical agitation, pushing of the particulates in the melt by using reciprocating rods, dispersion of the particulates by ultrasound are commonly used in the industry [3]. Nonetheless, the dispersion of the particulates in the melt using centrifugal acceleration is the method of choice when producing metal pipes, accounting for 15% of the total casting output of the world in terms of tonnage [4].

When a metal melt containing reinforcing particles is subjected to centrifugal force, a gradually varying particle enriched (matrix depleted) zone is formed during solidification. Depending on the density, the lighter particles segregate towards the axis of rotation, while the denser ones move away from axis of rotation. In the case of aluminum alloy, the particle enriched zone of heavier particles such as SiC, Al_2O_3 and $ZrSiO_4$ is at the outer boundary [5]. The gradient of particle segregation and volume fraction profiles along the thickness of the metal casting are related to the melt temperature, metal viscosity, cooling rate, the densities of the particle and liquid, particle size and magnitude of centrifugal acceleration [6].

Most papers in the literature on FGMs employ indiscriminately the rule of mixture or Mori-Tanaka schemes to obtain the effective material properties [7], [8] regardless of the constituents of the composite. However care must be taken when choosing the most appropriate micromechanical approach in order to accurately quantify the effect of the varying microstructure on the overall behavior of the material. In order to address this issue the present

work was divided into two main parts. Firstly a set of user material subroutines (UMATs) was developed for the Finite Element Analysis of the proposed problem. The code was later validated against analytical solutions for an FGM pressurized thick-wall cylinder with radially varying Young's modulus. Secondly a parametric study involving different volume fraction distributions and different homogenization schemes was carried out and discussed. The impact of these variables was assessed in terms of their influence on the radial and hoop stresses/strain profiles along the wall thickness.

2 MICROMECHANICS

A plethora of sound work exists for determining the effective properties of composite structures through the use of analytical micromechanics [9]–[12] and other semi-analytical, and finite element (FE) approaches [13]–[15]. These micromechanics models provide the necessary input to perform structural FE analysis based on the micro-scale properties using a "bottom-up" approach.

In the micromechanical homogenization schemes, the macroscopic equivalent parameters are obtained through the structural responses of representative volume elements (RVEs) which are defined on a finer scale. In this type of homogenization approach, a material point on the macroscopic level can be related to a representative volume element V on the microscopic level where stresses and strains prevail as varying micro-fields, assuming a statistically homogeneous distribution of the heterogeneities (inclusions) throughout the material. The macro-stresses and macro-strains which characterize the mechanical state of the macroscopic material point can be treated as volumetric averages of the microscopic fields over a certain volume V. These volumes must be chosen large enough to contain a certain number of inclusions, but small when compared to any length scale over which the average loading or deformation of the composite varies.

In the particular case of FGMs, the distribution of heterogeneities presents a spatial variation such that the condition of a statistically homogeneous microstructure is not observed and the use of effective properties must be understood simply as a reasonable estimate of the macro properties [16].

If the position vector is denoted by $\boldsymbol{x}$, the volume-averaged stresses and strains (represented by the brackets $\langle\ \rangle$), are defined as the average of the pointwise stress $\sigma_{ij}(\boldsymbol{x})$ and $\epsilon_{ij}(\boldsymbol{x})$ over the volume V:

$$\langle\sigma_{ij}\rangle = \frac{1}{V}\int_V \sigma_{ij}(\boldsymbol{x})dV \tag{1}$$

$$\langle\epsilon_{ij}\rangle = \frac{1}{V}\int_V \epsilon_{ij}(\boldsymbol{x})dV \tag{2}$$

It is convenient to define volume-averaged stresses and strain for the inclusions and matrix phases. Consider a two-phase composite consisting of an isotropic elastic matrix that occupies a volume $\mathrm{V_m}$ and an inclusion phase that occupies a volume $\mathrm{V_I}$ where the sum of these two volumes corresponds to the volume V and also consider that these two phases are perfectly bonded at their interfaces. The corresponding volume fractions of matrix and inclusions are given by $\mathrm{v_M} = \mathrm{V}_M/\mathrm{V}$ and $\mathrm{v_I} = \mathrm{V_I}/\mathrm{V} = 1 - \mathrm{v}_M$, respectively.

It follows that the average inclusion and matrix micro-fields (stress or strain) over the respective domains V_I and V_M are related by:

$$\langle\sigma_{ij}^{I}\rangle = \frac{1}{V_I}\int_{V_I}\sigma_{ij}(\boldsymbol{x})dV \;\; ; \;\; \langle\sigma_{ij}^{M}\rangle = \frac{1}{V_M}\int_{V_M}\sigma_{ij}(\boldsymbol{x})dV \tag{3}$$

$$\langle\epsilon_{ij}^{I}\rangle = \frac{1}{V_I}\int_{V_I}\epsilon_{ij}(\boldsymbol{x})dV; \;\; \langle\epsilon_{ij}^{M}\rangle = \frac{1}{V_M}\int_{V_M}\epsilon_{ij}(\boldsymbol{x})dV \tag{4}$$

The relationships between the matrix and inclusion averages and the overall averages can be defined in terms of the preceding definitions as:

$$\langle\sigma_{ij}\rangle = \mathrm{v}_f\langle\sigma_{ij}^{I}\rangle + \mathrm{v}_M\langle\sigma_{ij}^{M}\rangle = \mathrm{v}_I\langle\sigma_{ij}^{I}\rangle + (1-\mathrm{v}_I)\langle\sigma_{ij}^{M}\rangle \tag{5}$$

$$\langle\epsilon_{ij}\rangle = \mathrm{v}_f\langle\epsilon_{ij}^{I}\rangle + \mathrm{v}_M\langle\epsilon_{ij}^{M}\rangle = \mathrm{v}_I\langle\epsilon_{ij}^{I}\rangle + (1-\mathrm{v}_I)\langle\epsilon_{ij}^{M}\rangle \tag{6}$$

The Gauss' divergence theorem can be used to express these two macroscopic quantities by integrals over the boundary ∂V of the averaging domainV. It is assumed that the microscopic fields are differentiable throughout the entire domain, which does not hold true for heterogeneous materials with discontinuously varying properties.

Now consider that the volume V consists of two subdomains V_1 and $V_2$with different properties according to Figure 1. Consider also the interfacial surface between the two volumes as the boundary S.

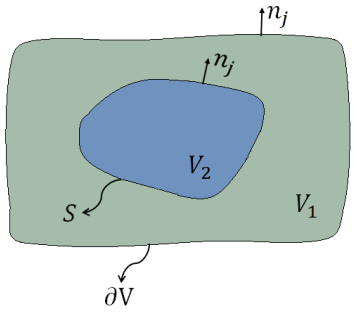

Figure 1 – Volume V with an internal interface S.

It can be seen that across the interface S, the stresses and displacements may not be differentiable. This challenge can be overcome if the divergence theorem is applied separately to the two subdomains where S appears, once as the boundary of V_2 (with outer unit normal n_j) and also as the inner boundary of V_1 (with outer unit normal $-n_j$). Considering the corresponding traction vectors of V_1 and V_2 as $t_i^{(1)}$ and $t_i^{(2)}$, respectively we have:

$$\langle\sigma_{ij}\rangle = \int_V \sigma_{ij}\,dV = \int_{V_1}\sigma_{ij}\,dV + \int_{V_2}\sigma_{ij}\,dV \rightarrow \int_{\partial V} t_i x_j dA + \int_S \left(t_i^{(2)} - t_i^{(2)}\right)x_j dA$$
$$\langle\sigma_{ij}\rangle = \int_{\partial V} t_i x_j dA \tag{7}$$

The equilibrium condition implies that $t_i^{(1)} = t_i^{(2)}$. As a result, for quasi-static problems, in the absence of body forces, the average stress in a given RVE is prescribed only in terms of the boundary traction and the macroscopic average quantities are valid regardless of the discontinuous material properties.

A similar expression for strain can also be developed if the strain tensor ϵ_{ij} is substituted by the corresponding displacement vector $\boldsymbol{u}$ into the definition of macrostrains (Equation 2). If the domain V is subjected to a surface displacement $\boldsymbol{u}(\boldsymbol{x})$, the divergence theorem can be applied:

$$\langle \epsilon_{ij} \rangle = \frac{1}{2V} \int_V \left(u_{i,j} + u_{j,i} \right) dV = \frac{1}{2V} \int_{\partial V} \left(u_i n_j + u_j n_i \right) dA \tag{8}$$

This is called the *average strain theorem* [17].

2.1 Eshelby Tensor

J. D. Eshelby developed a very important micromechanics solution for a specific class of inclusions inside an unbounded domain [10]. He considered an ellipsoidal inclusion, defined within the region Ω in an infinite homogeneous, isotropic, and elastic medium (matrix) undergoing a change in shape and size. He used the concept of eigenstrains (ϵ_{kl}^*) to prove that under the constraint of the matrix, the inclusion has an arbitrary homogeneous strain and stress fields. He proposed that the stress concentrated in an inhomogeneity can be equally represented as the stress concentrated by an inclusion undergoing an arbitrary type of transformation strain produced without external forces (eigenstrain). In this problem, the equilibrium strain and stress are to be determined in the case where a strain is prescribed in a certain volume within an infinitely large homogeneous material. The work of Toshio Mura is indicated as a further reading on the theory behind this model [18]. The strains inside the ellipsoidal inclusion are linearly related to the eigenstrains by the fourth order Eshelby tensor $\mathbb{S}_{ijkl}$, as follows:

$$\langle \epsilon_{ij}^I \rangle = \mathbb{S}_{ijkl} : \langle \epsilon_{kl}^* \rangle \tag{9}$$

This tensor presents the minor symmetry, but in general lacks the major symmetry:

$$\mathbb{S}_{ijkl} = \mathbb{S}_{jikl} = \mathbb{S}_{ijlk} \neq \mathbb{S}_{klij} \tag{10}$$

The geometry of an ellipsoidal inclusion Ω with semi axis a_i can be defined as:

$$\frac{x^2}{a_1^2} + \frac{y^2}{a_2^2} + \frac{z^2}{a_3^2} \leq 1 \tag{11}$$

Assuming $a_1 > a_2 > a_3$, the components of the Eshelby tensor are defined as

$$\begin{aligned} \mathbb{S}_{1111} &= \frac{3}{8\pi(1-v)} a_1^2 I_{11} + \frac{1-2v}{8\pi(1-v)} I_1 \\ \mathbb{S}_{1122} &= \frac{1}{8\pi(1-v)} a_2^2 I_{12} - \frac{1-2v}{8\pi(1-v)} I_1 \end{aligned} \tag{12}$$

$$\mathbb{S}_{1133} = \frac{1}{8\pi(1-v)} a_3^2 I_{13} - \frac{1-2v}{8\pi(1-v)} I_1$$

$$\mathbb{S}_{1212} = \frac{a_1^2 + a_2^2}{16\pi(1-v)} I_{12} + \frac{1-2v}{16\pi(1-v)} (I_1 + I_2)$$

All other non-zero components are obtained by cyclic permutation of (1, 2, 3). The components which cannot be obtained this way are zero [18]; for instance $\mathbb{S}_{1112} = \mathbb{S}_{1223} = \mathbb{S}_{1232} = 0$. The I_i can be expressed by standard elliptic integrals of the form:

$$I_1 = \frac{4\pi a_1 a_2 a_3}{(a_1^2 - a_2^2)\sqrt{a_1^2 - a_3^2}} \{F(\theta, k) - E(\theta, k)\}$$
$$I_3 = \frac{4\pi a_1 a_2 a_3}{(a_2^2 - a_3^2)\sqrt{a_1^2 - a_3^2}} \left\{ \frac{a_2\sqrt{a_1^2 - a_3^2}}{a_1 a_3} - E(\theta, k) \right\} \tag{13}$$

where

$$F(\theta, k) = \int_0^\infty \frac{1}{\sqrt{1 - k^2 sin^2(w)}} dw, \quad E(\theta, k) = \int_0^\infty \sqrt{1 - k^2 sin^2(w)}\, dw$$
$$\theta = \sqrt{arcsin(1 - a_3^2/a_1^2)}, \quad k = \sqrt{(a_1^2 - a_2^2)/(a_1^2 - a_3^2)}, \tag{14}$$

The remaining components are obtained by the following inter-relationships:

$$I_1 + I_2 + I_3 = 4\pi$$
$$3I_{11} + I_{12} + I_{13} = 4\pi/a_1^2$$
$$3a_1^2 I_{11} + a_2^2 I_{12} + a_3^2 I_{13} = 3I_1 \tag{15}$$
$$I_{12} = (I_2 + I_1)/(a_1^2 - a_2^2)$$

2.2 Mean-Field Homogenization

The multiscale method adopted in this work is the so called hierarchical method (also known as sequential method), where information is transmitted from the microscale to the macroscale in a straightforward way [19]. In a hierarchical approach, the micro-scale is modeled using an RVE, or unit cell, and is homogenized to determine the effective properties for use in an upper scale (meso or macro-scale) analysis.

The Mean-Field method is a well-known approach which is built upon the concept of an imaginary RVE. It accounts for the interaction subdomains pertinent to the various inclusions and finds the new averages that satisfy the boundary conditions [20]. As is typical for mean field micromechanics models, fourth-order concentration tensors relate the average stress or average strain tensors in inclusions and matrix to the average macroscopic stress or strain tensor, respectively.

Within the premises of the mean-field homogenization method, the per-phase average strains $\langle \epsilon_{ij} \rangle$ are related to one another by means of the strain concentration tensor. This tensor is essentially the ratio between the average inclusion strain and the corresponding average strain in the matrix:

$$\langle \epsilon_{kl}^{I} \rangle = B_{ijkl} : \langle \epsilon_{kl}^{M} \rangle \tag{16}$$

The per-phase average strains are related to the overall macrostrain by:

$$\langle \epsilon_{kl}^{M} \rangle = [v_I B_{ijkl} + (1 - v_I) I_{ijkl}]^{-1} : \langle \epsilon_{kl} \rangle \tag{17}$$

$$\langle \epsilon_{kl}^{I} \rangle = B_{ijkl} : [v_I B_{ijkl} + (1 - v_I) I_{ijkl}]^{-1} : \langle \epsilon_{kl} \rangle \tag{18}$$

where I designates the fourth order symmetric unit tensor. Different homogenization schemes will differ by the expression of B_{ijkl} , but in all of them the macro-stiffness tensor of the two phase composite is written as:

$$C_{ijkl} = \left[v_I C_{ijkl}^{I} : B_{klmn} + (1 - v_I) C_{ijkl}^{M} \right] : \left[v_I B_{klmn} + (1 - v_I) I_{ijkl} \right]^{-1} \tag{19}$$

where C_{ijkl}^{I} and C_{ijkl}^{M} are the inclusion and matrix stiffness, respectively.

Mean field homogenization schemes are relatively simple to implement within the framework of finite element codes and are very efficient from a computational standpoint. The homogenization schemes used in this work were implemented as Abaqus® custom subroutines to define the constitutive behavior of the material (UMATs). The methods used herein are briefly described as follows.

2.3 Voigt and Reuss Models

The two simplest homogenization schemes are the Voigt [21] and Reuss [22] models. The Voigt model is also known as Rule of Mixtures (RoM) and is based on the assumption of a uniform strain field within the RVE, which means that both matrix and inclusions are subjected to the same strain. It follows from this assumption that the strain concentration factor equals to the unit tensor, which yields the following expression when substituted in Equation 19:

$$B_{ijkl} = I_{ijkl}; \qquad C_{ijkl}^{voigt} = v_I C_{ijkl}^{I} + (1 - v_I) C_{ijkl}^{M} \tag{20}$$

This model can also be understood as a linearly weighted average of the properties of each phase. The Reuss model, on the other hand, assumes a uniform stress inside the RVE, meaning that all phases experience the same stress. This premise leads to a strain concentration factor that corresponds to the ratio between the stiffness of the matrix over the stiffness of the inclusion. Substituting the resulting strain concentration factor on Equation 19 one obtains:

$$B_{ijkl} = C_{ijkl}^{I^{-1}} : C_{klmn}^{M}; \qquad C_{ijkl}^{reuss} = \left[v_I C_{ijkl}^{I^{-1}} + (1 - v_I) C_{ijkl}^{M^{-1}} \right]^{-1} \tag{21}$$

Knowing that the inverse of the stiffness matrix corresponds to the compliance matrix $(C_{ijkl}^{-1} = S_{ijkl})$, the Equation 21 can be similarly expressed as:

$$S_{ijkl}^{reuss} = v_I S_{ijkl}^{I} + (1 - v_I) S_{ijkl}^{M} \tag{22}$$

Those two models are too far apart from each other and do not take into account the shape or the orientation of the inclusions. Moreover, the interaction between inclusions inside

the matrix is not accounted for, which renders the two schemes useless for medium to high concentration of inclusions. However, the two models serve the purpose of setting the extreme (upper and lower) boundaries where the other models must lay inside.

2.4 Mori-Tanaka Model

Except for Reuss and Voigt models, all the other mean field homogenization schemes are based on the fundamental work of Eshelby [10]. The Mori-Tanaka model [11] is one of the most prominent models in this category. In their original paper, Mori and Tanaka treated the problem of homogeneous inclusions.

As is typical for mean field micromechanics models, fourth-order concentration tensors relate the average stress or average strain tensors in inhomogeneities and matrix to the average macroscopic stress or strain tensor, respectively; inhomogeneity "feels" effective matrix fields, accounting for phase interaction effects in a collective, approximate way.

The Mori-Tanaka homogenization scheme considers the strain concentration tensor to be equal to that of a single inclusion problem, which in turn means that the inclusions in the RVE, experience the matrix strain as the far-field strain in the Eshelby theory. The strain concentration tensor in Mori-Tanaka's model is given by:

$$B_{ijkl} = H_{ijkl}^{MT} = (I_{ijkl} + \mathbb{S}_{klmn} : \left[{C_{ijkl}^{M}}^{-1} : C_{klmn}^{I} - I_{ijkl} \right])^{-1} \tag{23}$$

The homogenized macro stiffness is obtained by substituting Equation 23 into 19 [12]:

$$C_{ijkl}^{MT} = I_{ijkl} + \mathbb{S}_{klmn} : \left[{C_{ijkl}^{M}}^{-1} : C_{klmn}^{I} - I_{ijkl} \right])^{-1} \tag{24}$$

2.5 Self-Consistent Model

The Self-Consistent homogenization scheme has been originally developed to estimate the equivalent stiffness of polycristals and take into account the interaction of the matrix and the grains following Eshelby's formulation. This approach was originally proposed by Hill [17], [23] and focused on spherical particles and continuous aligned fibers.

The Self-Consistent approach to homogenization is based upon the idea that the existence of a single inhomogeneity does not affect the effective material properties in a system with many inclusions. Therefore, the inclusions interact with each other through the effective medium, which means that the localization tensors will be based on the effective medium properties rather than the matrix material properties [24]. Conversely, the local interaction of the inclusions with the surrounding matrix material remains unaltered.

Self-Consistent models are also referred to as embedding models, because the properties of the composite are assumed to be the same as the averaged properties of a single particle embedded into an infinite matrix with a given stiffness C_{ijkl}. Of course these properties are initially unknown; however, numerical solutions are easily obtained by an iterative algorithm. The Self-Consistent strain concentration tensor is given by:

$$B_{ijkl} = H_{ijkl}^{SC} = \left[I_{ijkl} + S_{ijkl} : \left(C_{klmn}^{-1} : C_{mnop}^{f} - I_{ijkl} \right) + I_{ijkl} \right]^{-1} \tag{25}$$

The Self-Consistent method is known to overestimate the influence of the interaction among the inclusions, especially for softer matrices [25]. Christensen and Lo [26] proposed an improved methodology to address this issue and make it yield the correct asymptotic behavior for rigid inclusions as its volume fraction approaches 100%. This scheme was named Generalized Self-Consistent Method and considers that the particulate phase is first surrounded by some matrix material and then embedded in the effective medium [24]. As the Generalized Self-Consistent Method is widely regarded as superior when compared to the original approach [27], it was adopted in this study.

3 UMAT DEVELOPMENT AND VALIDATION

In order to conduct the Finite Element Analysis of the FGM pressurized pipe in Abaqus®, a user material subroutine (UMAT) was developed. The main purpose was to code the various homogenization schemes as well as to allow for the possibility of using different Eshelby tensors for different shapes and aspect ratios. The first step towards this goal was to make sure that the stresses and strains obtained by the UMAT, given a pre-established modulus profile, were in accordance with the analytical solutions available for this type of problem. This was done prior to the implementation of the actual homogenization schemes and relied upon an already homogenized radial variation of the Young's modulus along the pipe wall. At this stage the UMAT would get the three Cartesian coordinates of each Gauss (integration) point passed on by Abaqus, and transform it to cylindrical coordinates. The homogenized modulus, at each Gauss point, was then obtained by the designated equation for the Young's modulus as a function of radial position. Finally, the three-dimensional stiffness and consistent matrices were assembled and the stress vector calculated.

A set of analytical solutions found in the literature was used in this work to verify the accuracy of the numerical results. The analytical expressions for radial hoop stresses were given by Li and Peng [28] for an FGM cylinder with an inner radius a, and outer radius b, subjected to an internal pressure p_i. The authors assumed a fixed Poisson's ratio, $v(r) = v$, and established that the Young's modulus varied radially according to a power law given by:

$$E(r) = E_0 \left(\frac{r}{b}\right)^{\beta} \tag{27}$$

The expressions for radial and hoop stresses are respectively:

$$\sigma_r(r) = -p \left(\frac{a}{r}\right)^{(2+k-\beta)/2} \frac{b^k - r^k}{b^k - a^k}$$

$$\sigma_\theta(r) = p \left(\frac{a}{r}\right)^{(2+k-\beta)/2} \frac{1}{b^k - a^k} \left[\frac{2-(\beta+k)v}{\beta+k-2v} b^k - \frac{2-(\beta-k)v}{\beta-k-2v} r^k\right] \tag{28}$$

$$k = \sqrt{\beta^2 + 4 - 4\beta v}$$

The finite element model consisted of ¼ of a cylindrical section subjected to an internal pressure and with a traction-free outer surface. It had 200 mm in height and the inner and outer radius were, a = 100 and b = 150 mm respectively. The wall thickness was discretized using 10 elements and employed the 20 node quadratic element with reduced integration (C3D20R). An internal pressure of 10 MPa was applied at the inner surface of the cylinder, while no boundary

conditions were imposed on the outer surface. The model and the radial stress field can be seen in Figure 2.

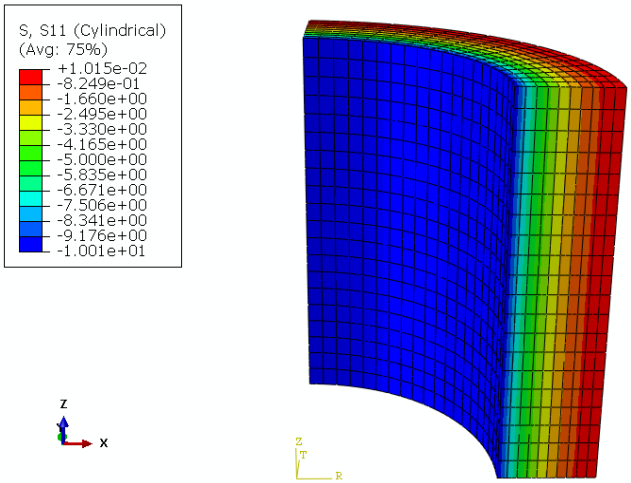

Figure 2 – Finite element radial stresses.

The numerical results for three different values of the exponent β (equation 27) were compared with results from Equation 28. The normalized radial and hoop stress profiles are given in Figures 3 and 4.

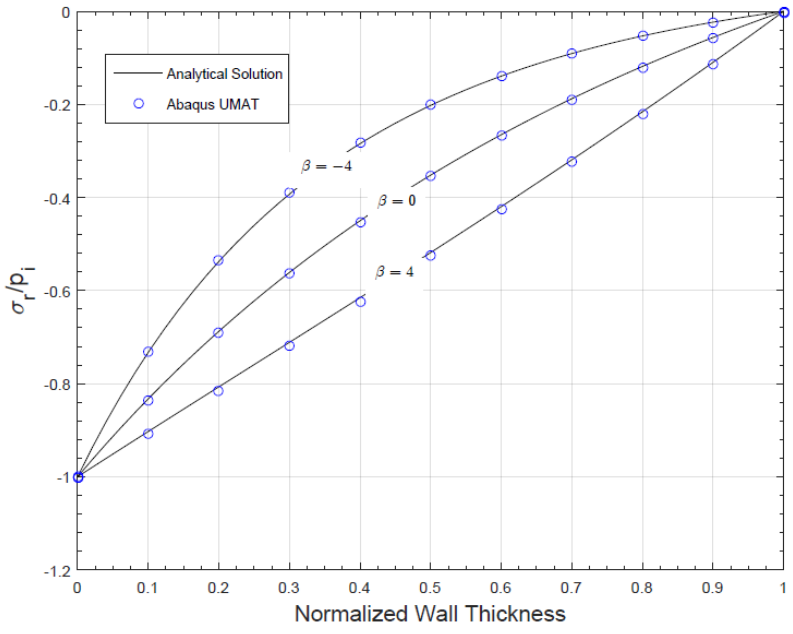

Figure 3 – Radial stress profiles along the pipe wall.

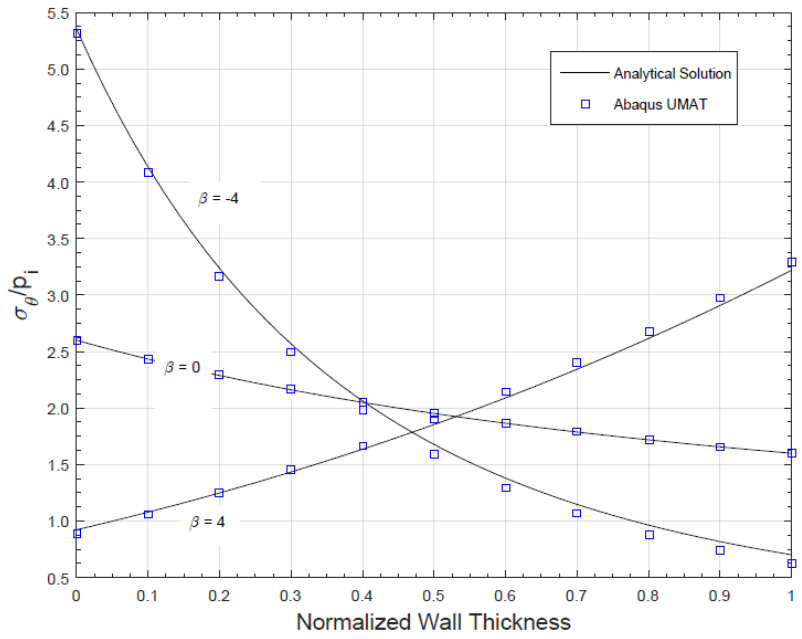

Figure 4 – Hoop stress profiles along the pipe wall.

The results were deemed satisfactory in spite of minor differences on the hoop stresses. This is believed to be caused by the boundary conditions of the finite element model, which had no radial constraints at the top and bottom faces. The analytical model, on the other hand, was based on a plane strain configuration.

3.1 Implementation of the Homogenization Schemes

The next step on the development of the UMATs was to implement the various homogenization schemes discussed in this study. In order to establish a baseline for comparison among all models, several experimental studies on Al/SiC MMCs were compiled [29][30][31][32][33][34], and presented in Figure 5. The studies encompassed various volume fractions of SiC ranging from 0% to a little over 75%. It is worth noting that these studies used different aluminum alloys and SiC particles with various gradations.

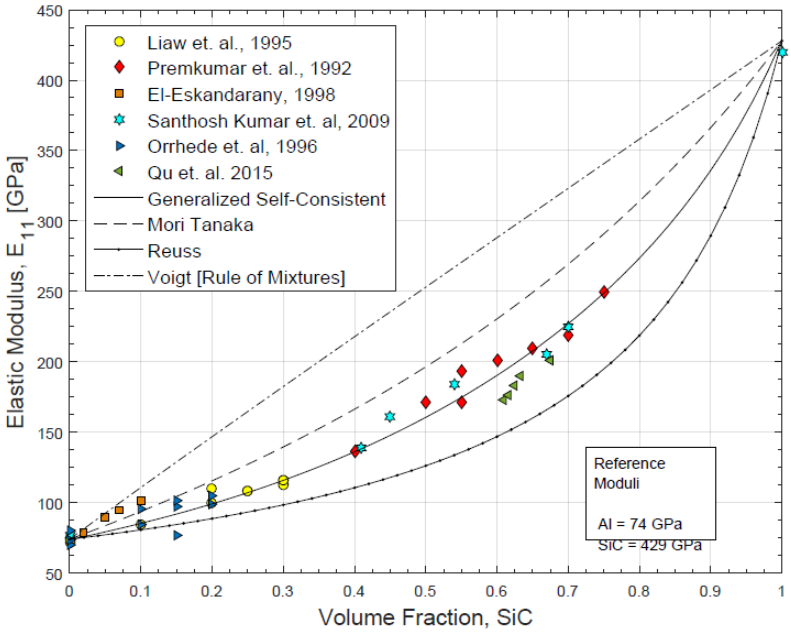

Figure 5 – Comparison of various homogenization schemes against experimental data.

The four homogenization schemes in discussion here were firstly implemented as Fortran standalone programs in order to check for any errors prior to the implementation as subroutines within the UMAT. This effort also served the purpose of showing which model ranked best among the four over various volume fraction ranges (low medium and high concentrations). This is important because the effective measurement of the Young's modulus along the thickness of an FGM is very difficult to achieve, whereas the measurement of the volume fraction distribution along the same thickness is more amenable from an experimental standpoint.

One important thing to be noted here is that, despite its enormous popularity, the use of the Voigt model (rule of mixtures) to predict the homogenized modulus of Al/SiC MMCs must be avoided. From this dataset, it is also pondered that the Generalized Self-Consistent seems to be the most suited model for this type of material. The Mori-Tanaka only provided reasonable results up to 20%. This is a well-known characteristic of this model and arises from the fact that it is based on a dilute assumption where the interference between adjacent inclusions is neglected. The four homogenization schemes were then coded as UMATs, one for each model and used in the parametric study described as follows.

4 PARAMETRIC STUDY

The volume fraction profiles in FGMs are usually approximated by well-defined functions such as exponentials, power-laws, sigmoidal functions as well as linearly varying distributions. The use of a parametric form to represent the volume fraction profiles is fundamental to establish the right quantities of each phase at any given point along the axis where the properties vary. However those functions must reflect the actual distribution of inclusions along the wall thickness, and in many cases simple functions are not able to represent well the measured data.

The parametric study was based upon the volume fraction profile obtained from Rajan et al, 2010 [35] shown in Figure 6. The experimental data was fitted to an exponential and a B-Spline curve so as to quantify the divergences when assuming a simpler curve (exponential) comparatively to a curve that represents better the measured data. The UMATs corresponding to each homogenization scheme were used for calculation of the hoop and radial stresses along the wall thickness.

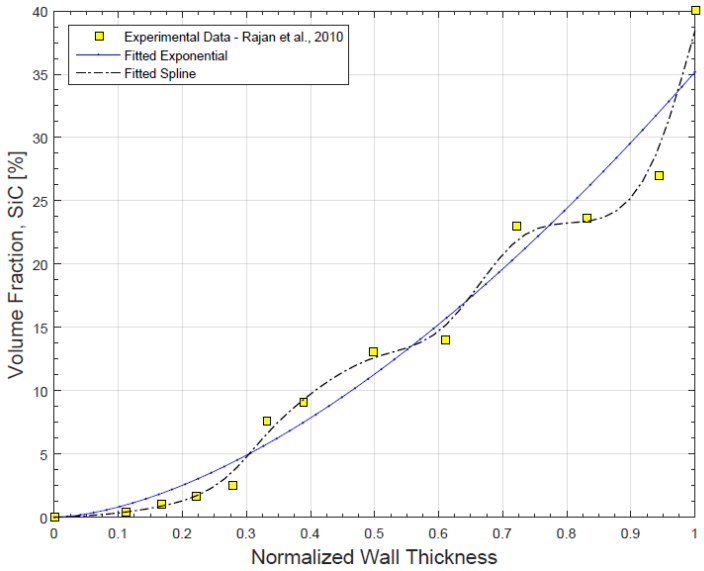

Figure 6 – Different fitted curves to the experimental data.

The Generalized-Self Consistent method was used to provide the comparison between the B-Spline fitted curve and the exponential fitted one. Figure 7 shows the results obtained using the two functions. No substantial differences are observed in terms of radial stress.

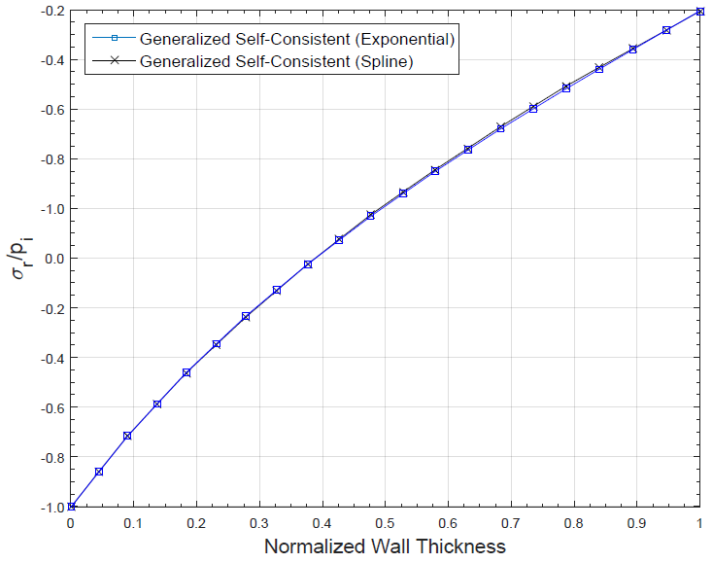

Figure 7 – Radial stress profiles for different representations of the volume fraction distribution.

In the case of hoop stresses (Figure 8), the overall trend is captured by both curves; however there are major differences between the results from the two approaches. The "waviness" of the volume fraction distribution reflects directly on the calculated stress when the actual volume fraction profile is taken into account. This is an important fact to be considered when employing an FGM material because it defeats the idea that the material is free of stress concentrations due to abrupt changes in stiffness.

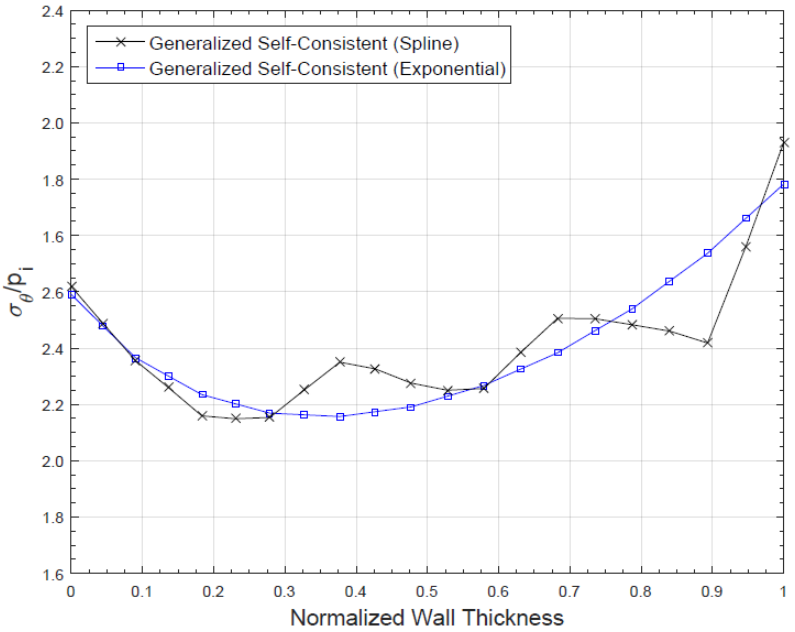

Figure 8 – Hoop stress profiles for different representations of the volume fraction distribution.

These results were further investigated and the influence of the homogenization method was assessed. The same B-Spline function was used in all four homogenization schemes and the results are presented in Figure 9. As can be seen, the homogenization scheme also plays a major role on the final results of hoop stresses. In the case of the Voigt model, the stresses calculated at the inner surface of the wall were higher than the stresses on the outer surface, contradicting the other models. The results show the critical role the homogenization schemes play on mechanical analysis of thick-walled FGM structures.

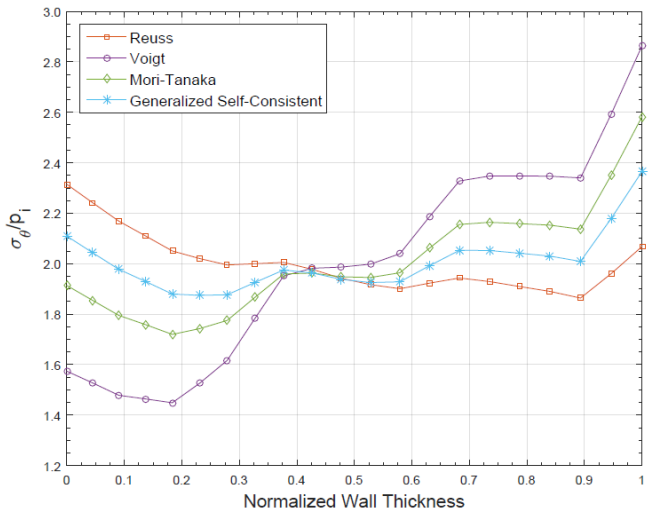

Figure 9 – Normalized hoop stress from various homogenization methods.

5 CONCLUDING REMARKS

This work was aimed at investigating the influences of different forms of volume fraction description as well as the impact of using different homogenization schemes on the overall behavior of a FGM pressurized hollow cylinder. To achieve this goal, a set of user-material subroutines were developed and implemented into Abaqus. They were used to simulate an FGM pressurized pipe, where the volume fraction of the SiC particulate was precisely measured. The results obtained showed the importance of correctly describing the distribution of the particulate reinforcement (volume fraction of inclusions) along the wall thickness. An assumption of an exponential variation may lead to unrealistic hoop stress distributions along the radial profile of the structural element. It may also mask potential issues related to stress concentration in some areas were the volume fraction concentration does not varies as smoothly as predicted by simple functions, such as exponential, power-laws and so forth. The tools and analysis methodology developed in this paper are also expected to improve the understanding of FGM material behavior and the importance on quality control on the production of such materials.

ACKNOWLEDGMENTS

The authors acknowledge the financial support provided by CNPq (Conselho Nacional de Desenvolvimento Científico e Tecnológico).

REFERENCES

[1] K. U. Kainer, *Metal Matrix Composites: Custom-made Materials for Automotive and Aerospace Engineering*, 1st Editio. Verlag, Wiley-VCH, 2006.

[2] M. Koizumi, “FGM activities in Japan,” *Compos. Part B Eng.*, vol. 28, no. 1–2, pp. 1–4, Jan. 1997.

[3] P. S. Bains, S. S. Sidhu, and H. S. Payal, "Fabrication and Machining of Metal Matrix Composites: A Review," *Mater. Manuf. Process.*, vol. 31, no. 5, pp. 553–573, Apr. 2016.

[4] *ASM Handbook Volume 15: Casting*, First Edit. ASM International, 2008.

[5] E. Jayakumar, J. C. Jacob, T. P. D. Rajan, M. A. Joseph, and B. C. Pai, "Processing and Characterization of Functionally Graded Aluminum (A319)—SiCp Metallic Composites by Centrifugal Casting Technique," *Metall. Mater. Trans. A*, vol. 47, no. 8, pp. 4306–4315, Aug. 2016.

[6] Y. Watanabe and S. Oike, "Formation mechanism of graded composition in Al–Al2Cu functionally graded materials fabricated by a centrifugal in situ method," *Acta Mater.*, vol. 53, no. 6, pp. 1631–1641, Apr. 2005.

[7] H.-S. Shen and Z.-X. Wang, "Assessment of Voigt and Mori–Tanaka models for vibration analysis of functionally graded plates," *Compos. Struct.*, vol. 94, no. 7, pp. 2197–2208, Jun. 2012.

[8] A. H. Akbarzadeh, A. Abedini, and Z. T. Chen, "Effect of micromechanical models on structural responses of functionally graded plates," *Compos. Struct.*, vol. 119, pp. 598–609, Jan. 2015.

[9] X. Peng, S. Tang, N. Hu, and J. Han, "Determination of the Eshelby tensor in mean-field schemes for evaluation of mechanical properties of elastoplastic composites," *Int. J. Plast.*, vol. 76, pp. 147–165, 2016.

[10] J. D. Eshelby, "The Determination of the Elastic Field of an Ellipsoidal Inclusion, and Related Problems," *Proc. R. Soc. A Math. Phys. Eng. Sci.*, vol. 241, no. 1226, pp. 376–396, Aug. 1957.

[11] T. Mori and K. Tanaka, "Average stress in matrix and average elastic energy of materials with misfitting inclusions," *Acta Metall.*, vol. 21, no. 5, pp. 571–574, May 1973.

[12] Y. Benveniste, "A new approach to the application of Mori-Tanaka's theory in composite materials," *Mech. Mater.*, vol. 6, no. 2, pp. 147–157, Jun. 1987.

[13] W. Tian, L. Qi, J. Zhou, J. Liang, and Y. Ma, "Representative volume element for composites reinforced by spatially randomly distributed discontinuous fibers and its applications," *Compos. Struct.*, vol. 131, pp. 366–373, Nov. 2015.

[14] I. Doghri and L. Tinel, "Micromechanical modeling and computation of elasto-plastic materials reinforced with distributed-orientation fibers," *Int. J. Plast.*, vol. 21, no. 10, pp. 1919–1940, Oct. 2005.

[15] Y. Huang, L. Xu, and S. Kyu Ha, "Prediction of three-dimensional composite laminate response using micromechanics of failure," *J. Compos. Mater.*, vol. 46, no. 19–20, pp. 2431–2442, Sep. 2012.

[16] D. Gross and T. Seelig, *Fracture Mechanics*. Berlin, Heidelberg: Springer Berlin Heidelberg, 2011.

[17] R. Hill, "Theory of mechanical properties of fibre-strengthened materials: I. Elastic behaviour," *J. Mech. Phys. Solids*, vol. 12, no. 4, pp. 199–212, Sep. 1964.

[18] T. Mura, *Micromechanics of defects in solids*. Dordrecht: Springer Netherlands, 1982.

[19] T. Belytschko and J.-H. Song, "Coarse-graining of multiscale crack propagation," *Int. J. Numer. Methods Eng.*, vol. 81, no. 5, pp. 537–563, 2010.

[20] E. S. Perdahcıoğlu and H. J. M. Geijselaers, "Constitutive modeling of two phase materials using the mean field method for homogenization," *Int. J. Mater. Form.*, vol. 4, no. 2, pp. 93–102, Jun. 2011.

[21] W. Voigt, "Ueber die Beziehung zwischen den beiden Elasticitätsconstanten isotroper Körper," *Ann. Phys.*, vol. 274, no. 12, pp. 573–587, 1889.

[22] A. Reuss, "Berechnung der Fließgrenze von Mischkristallen auf Grund der Plastizitätsbedingung für Einkristalle .," *ZAMM - Zeitschrift für Angew. Math. und Mech.*, vol. 9, no. 1, pp. 49–58, 1929.

[23] R. Hill, "Theory of mechanical properties of fibre-strengthened materials—III. self-consistent model," *J. Mech. Phys. Solids*, vol. 13, no. 4, pp. 189–198, Aug. 1965.

[24] R. M. Christensen, *Theory of Viscoelasticity*, 2nd Ed. New York: Academic Press, Inc, 1982.

[25] Y. Huang, K. X. Hu, X. Wei, and A. Chandra, "A generalized self-consistent mechanics method for composite materials with multiphase inclusions," *J. Mech. Phys. Solids*, vol. 42, no. 3, pp. 491–504, Mar. 1994.

[26] R. M. Christensen and K. H. Lo, "Solutions for effective shear properties in three phase sphere and cylinder models," *J. Mech. Phys. Solids*, vol. 27, no. 4, pp. 315–330, Aug. 1979.

[27] C. L. Tucker III and E. Liang, "Stiffness predictions for unidirectional short-fiber composites: Review and evaluation," *Compos. Sci. Technol.*, vol. 59, no. 5, pp. 655–671, Apr. 1999.

[28] X. L. X. Peng, "A Pressurized Functionally Graded Hollow Cylinder with Arbitrarily Varying Material Properties," pp. 81–95, 2009.

[29] P. K. Liaw, R. E. Shannon, W. G. Clark, W. C. Harrigan, H. Jeong, and D. K. Hsu, "Nondestructive characterization of material properties of metal-matrix composites," *Mater. Chem. Phys.*, vol. 39, no. 3, pp. 220–228, Jan. 1995.

[30] M. K. Premkumar, W. H. Hunt, and R. R. Sawtell, "Aluminum composite materials for multichip modules," *JOM*, vol. 44, no. 7, pp. 24–28, Jul. 1992.

[31] M. Sherif El-Eskandarany, "Mechanical solid state mixing for synthesizing of SiCp/Al nanocomposites," *J. Alloys Compd.*, vol. 279, no. 2, pp. 263–271, Oct. 1998.

[32] S. Santhosh Kumar, V. Seshu Bai, K. V Rajkumar, G. K. Sharma, T. Jayakumar, and T. Rajasekharan, "Elastic modulus of Al–Si/SiC metal matrix composites as a function of volume fraction," *J. Phys. D. Appl. Phys.*, vol. 42, no. 17, p. 175504, Sep. 2009.

[33] M. Orrhede, R. Tolani, and K. Salama, "Elastic Constants and Thermal Expansion of Aluminum-SiC Metal-Matrix Composites," *Res. Nondestruct. Eval.*, vol. 8, no. 1, pp. 23–37, Jan. 1996.

[34] S. Qu, H. Lou, and X. Li, "Influence of particle size distribution on properties of SiC particles reinforced aluminum matrix composites with high SiC particle content," *J. Compos. Mater.*, vol. 50, no. 8, pp. 1049–1058, Apr. 2016.

[35] T. P. D. Rajan, R. M. Pillai, and B. C. Pai, "Characterization of centrifugal cast functionally graded aluminum-silicon carbide metal matrix composites," *Mater. Charact.*, vol. 61, no. 10, pp. 923–928, Oct. 2010.